Title
Kinetics of moisture-induced phase transformation in inorganic halide perovskite

Journal
Matter, 4(7)

ISSN
2590-2393

Authors
Lin, Zhenni
Zhang, Ye
Gao, Mengyu
et al.

Publication Date
2021-07-01

DOI
10.1016/j.matt.2021.04.023

Peer reviewed

Kinetics of moisture-induced phase transformation in inorganic halide perovskite

ZhenniLin, YeZhang, Mengyu Gao, Julian A.Steele, SheenaLouisia,SunmoonYu, Li NaQuan, Chung-KuanLin, David T.Limmer,PeidongYang

The high-temperature (high-T) phase of cesium lead iodide ($CsPbI_3$) presents great promise for photovoltaic applications; however, exposure to ambient moisture at room temperature transforms it into its less-desirable low-temperature (low-T) phase with a larger band gap. While there have been theoretical predictions on the influence of moisture level on the phase transformation kinetics, the corresponding quantitative experimental evidence has remained limited. Tracking $CsPbI_3$ phase transformation under controlled relative humidity (RH), we find that rising RH increases the nucleation rate of low-T $CsPbI_3$ exponentially, but has a weak effect on its growth. The overall transformation is nucleation limited, with higher RH leading to a lower nucleation barrier. Finally, we find that heating between 40°C and 80°C facilitates water desorption and suppresses phase transformation. Our findings elucidate the relationship between moisture and the phase energetics of $CsPbI_3$, which can serve as references for thin film applications of $CsPbI_3$ and future designs of stable photovoltaics systems.

Introduction

The high-temperature, perovskite phase of cesium lead iodide (high-T $CsPbI_3$) is promising for efficient, next-generation low-cost solar cells due to its high photoconversion efficiency,[1] low processing cost,[2,3] and enhanced thermal stability compared with its organic-based counterparts[4, 5, 6]; however, it can only exist in a metastable perovskite phase below 310°C if the appropriate synthetic steps are taken.[4,7, 8, 9, 10, 11, 12] Upon exposure to moisture, metastable high-T $CsPbI_3$ (band gap ~1.73 eV) tends to transform into a thermodynamically preferred low-temperature (low-T), non-perovskite phase[4,10,13,14] (Figure 1A), which has a wider band gap (~2.82 eV) and lower photoconversion efficiency, rendering it unsuitable for optoelectronic applications. Therefore, a foundational understanding of how moisture influences the phase transformation (PT) kinetics is critical to the development of ambient-stable $CsPbI_3$ photovoltaic cells.

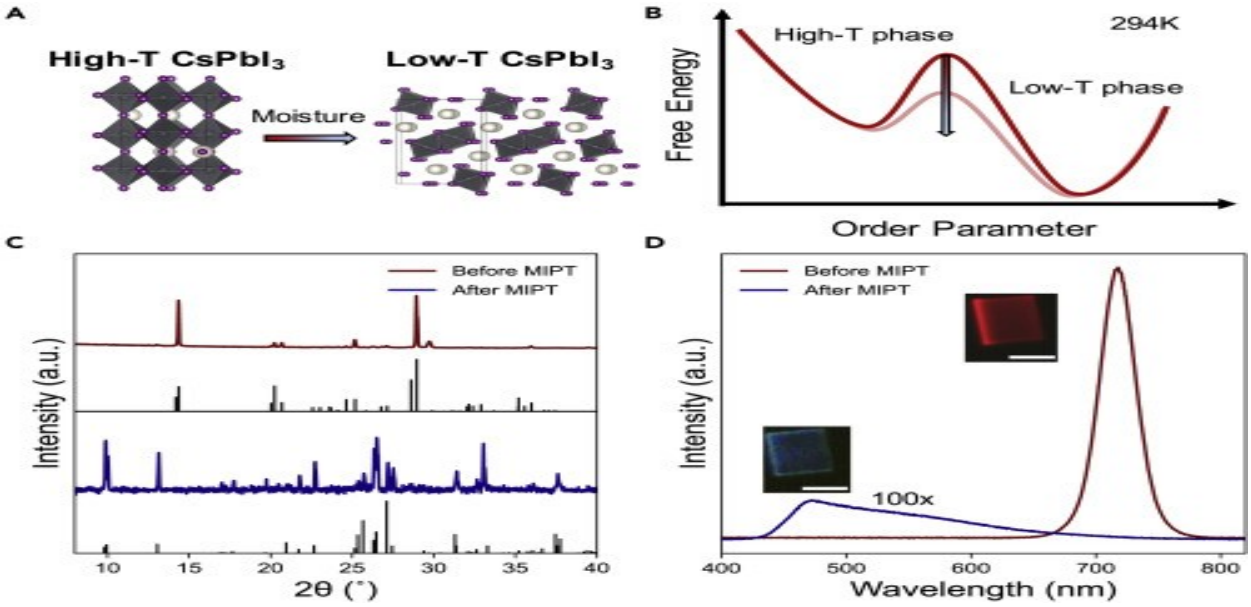

Figure 1. Moisture-induced phase transformation of $CsPbI_3$

(A) Schematic diagrams of high-T $CsPbI_3$ (left, orthorhombic structure with three-dimensionally connected corner-sharing octahedra) to low-T $CsPbI_3$ (right, orthorhombic structure with one-dimensional chains of edge-sharing octahedra) phase transformation triggered by moisture. Cesium, lead (inside the $[PbI_6]^{4-}$ octahedra), and iodide atoms are shown in white, gray, and purple, respectively. Unit cells are delineated by black solid lines.
(B) Illustrative energy diagram of $CsPbI_3$ (thick red line) comparison with common moisture-induced modification (faint red line) of the energy scheme.
(C) Powder X-ray diffraction of $CsPbI_3$ before and after moisture-induced phase transformation (MIPT). Black bar graphs represent reference spectra for the metastable γ-phase $CsPbI_3$ (top), and the stable δ-phase $CsPbI_3$ (bottom), obtained from Sutton et al.[15]
(D) Photoluminescence (laser excitation: 375 nm) spectra and images (inset) of $CsPbI_3$ before and after MIPT. Scale bars, 10 μm.

Molecular dynamics simulations[16] predict that, when a thin water layer is in contact with the metastable perovskite surface, it enhances the halide vacancies at the water-perovskite interface due to the large solvation enthalpy of halide ions and their accompanying low vacancy formation energy. The halide vacancies can be considered as defect sites that lower the PT barrier between the metastable high-T phase and the stable low-T phase of $CsPbI_3$ (Figure 1B), effectively catalyzing the transformation. After a monolayer of water has formed on the surface of high-T $CsPbI_3$, a further increase in RH leads to an exponential increase in the equilibrium concentration of vacancies, which can be assumed to be proportional to the larger heterogeneous nucleation rate relative to the homogeneous rate in a simple nucleation model. Therefore, based on the prediction, rising RH level should lead to an exponential increase in the nucleation rate of low-T phase $CsPbI_3$. However, there is yet to be an experimental study of incremental "ambient moisture"—an ambiguous term that can range from 20% to 80% depending on geographical location and time of the year—to shed light on the underlying relationship in $CsPbI_3$.

To quantitatively describe the influence of moisture in PT kinetics, we must first capture the time evolution of PT to understand the reaction mechanism under varying RH levels. Reaction mechanism reflects how the transformation rate changes based on the concentration of the high-T phase.[17] Any changes in a system's interaction with the catalyst over time will manifest as deviations in the transformation rate from a simple nucleation model. Existing kinetic studies of $CsPbI_3$, or its related compositions, have mainly focused on the impact of moisture on the total time needed to reach transformation,[13,16,18] but not on the impacts as related to the specific variations of PT rate over time. Consequently, any changes in the reaction kinetics due to secondary reactions would have been obscured, and the dominant PT process, i.e., phase nucleation in comparison with phase growth, cannot be decoupled. Experimental studies of moisture-induced phase transformation (MIPT) kinetics have thus far involved either polycrystalline thin films[13,16] or nanocrystals,[18] both of which are morphologies that unavoidably convolve nucleation and growth. For instance, in thin films, the MIPT of one grain can overlap with a secondary nucleation in the same or a neighboring grain, thereby obscuring the kinetics. In nanocrystals, the growth may proceed too rapidly for its evolution to be captured. As a result, the influence of moisture on each individual PT process, as well as the rate-limiting step, are unknown.
Here, we study the high-T (perovskite) to low-T (non-perovskite) PT kinetics in individual $CsPbI_3$ microcrystals (5–15 μm in average lateral dimension) using *in situ* photoluminescence (PL) and optical microscopy, effectively identifying the reaction mechanism and the rate-limiting step. Humidity control reveals two distinct regimes for the MIPT kinetics: transformation of high-T crystals that follows a single exponential decay below 83% RH, and the emergence of a secondary reaction that accelerates the process above 83% RH. The nucleation rate, J_N, is observed to increase exponentially with rising RH, which is consistent with previous predictions made by molecular dynamic simulations.[16] After nucleation, low-T growth proceeds with a weak linear dependence on RH. While nucleation can take up to a few hours to initiate, the growth of the low-T phase within a single crystal is completed within a minute, which indicates that nucleation is the rate-limiting step in MIPT. The activation energy barrier for nucleation (E_a) is estimated for two different RH levels: 55.40 ± 3.75 kJ/mol at 73% RH, 129.08 ± 33.86 kJ/mol at 53% RH. In addition, heating at 40°C–85°C can counteract the effect of moisture through water desorption, resulting in relatively lower J_N values at elevated temperatures. These findings elucidate the influence of environmental stressors on the phase stability of $CsPbI_3$ and provide insights to not only the stability of $CsPbI_3$ and its related compositions, but also more generally the kinetics of metastable to stable PT in crystalline materials.

Results and discussion

We used chemical vapor transport to directly synthesize high-T $CsPbI_3$ microcrystals (experimental procedures/supplemental information). The resultant crystals exhibit regular facets (Figure S1A) and a distinct red PL emission (Figure S1B), with powder X-ray diffraction confirming an orthorhombic perovskite-phase structure (γ-phase)[15] before MIPT (Figure 1C, top) and non-perovskite-phase orthorhombic structure (δ-phase)[15] after MIPT (Figure 1C, bottom). The PL emissions of $CsPbI_3$ before

and after the transformation center at 718 nm (1.73 eV) and 472 nm (2.63 eV), respectively (Figure 1D).

We tracked the nucleation behavior of low-T $CsPbI_3$ in MIPT under well-controlled RH (52%–90%) (experimental procedures) to quantify the influence of moisture on nucleation rate. Probability distribution of nucleation over time reveals that nucleation generally follows a first-order reaction kinetics, with rates rising exponentially with RH. Figure 2A and Video S1 display time evolution of high-T to low-T PT at 90% RH over the course of 1 h and 45 min. A 375 nm continuous-wave laser (wide field) is used to excite the crystals, and an optical microscope is used to simultaneously collect the PL emission. Due to their contrasting emission colors, high-T phase $CsPbI_3$ can be easily distinguished from low-T $CsPbI_3$. The number of fully transformed crystals is marked by the disappearance of red emission (high-T phase indicator) and the emergence of blue emission (low-T phase indicator). Representative emission images for all other RH levels are shown in Figures S2. The high-T to low-T nucleation times at the aforementioned RH levels (Figure 2B, inset) are used to construct the probability distribution of nucleation fraction over time (Figures 2B and S3). Higher RH is shown to correlate with a greater fraction of nucleation events within the same time interval across each dataset. The nucleation kinetics for RH lower than 83% follows first-order kinetics as a result of the Poisson distribution[17] (supplemental information), which is used to describe nucleation with the following assumption: the appearance of a critical nucleus is (1) a random process under a constant supersaturation, which, in this case, would be the presence of high-T phase in each untransformed crystal, and (2) is independent from another critical nuclei. The probability of nucleation over time, $P(t_J)$ is described using the following equation: $P(tJ)=1-\exp(-JN*tJ)$, where J_N is the stationary nucleation rate for a microcrystal within time, t_J. The close fitting (Table S1; Figure S4) of single exponential decay derived from Poisson distribution is reasonable, because the following conditions have been met: (1) there is a constant supersaturation of high-T phase in each individual untransformed crystal and (2) the crystals are physically distanced from each other such that transformation of one does not affect that of another. On the other hand, the nucleation kinetics for 83% and 90% shows clear deviation from the first-order kinetics over time (Figure S5); a secondary reaction emerges around 90 min for 90% RH, and 135 min for 83% RH, further increasing J_N. We attribute the sudden increase in J_N to water microdroplet formation (Figure S6) on the surface of crystals, which is not observed at RH below 81% (Figure S7). Thus, J_N values for 90% RH and 83% RH are extracted before the emergence of the water microdroplet using the aforementioned equation (Table S1; Figure S5). Table S2 lists a summary of J_N values at various RH. We find that J_N grows exponentially with rising RH (Figure 2C), confirming the previous theoretical predictions.[16] Microscopically, the observed relationship can be explained by the fact that increasing RH provides more driving force for iodide ions to migrate toward the water layer, which results in a larger amount of iodide vacancies in the perovskite lattice that eventually leads to an enhanced nucleation rate.

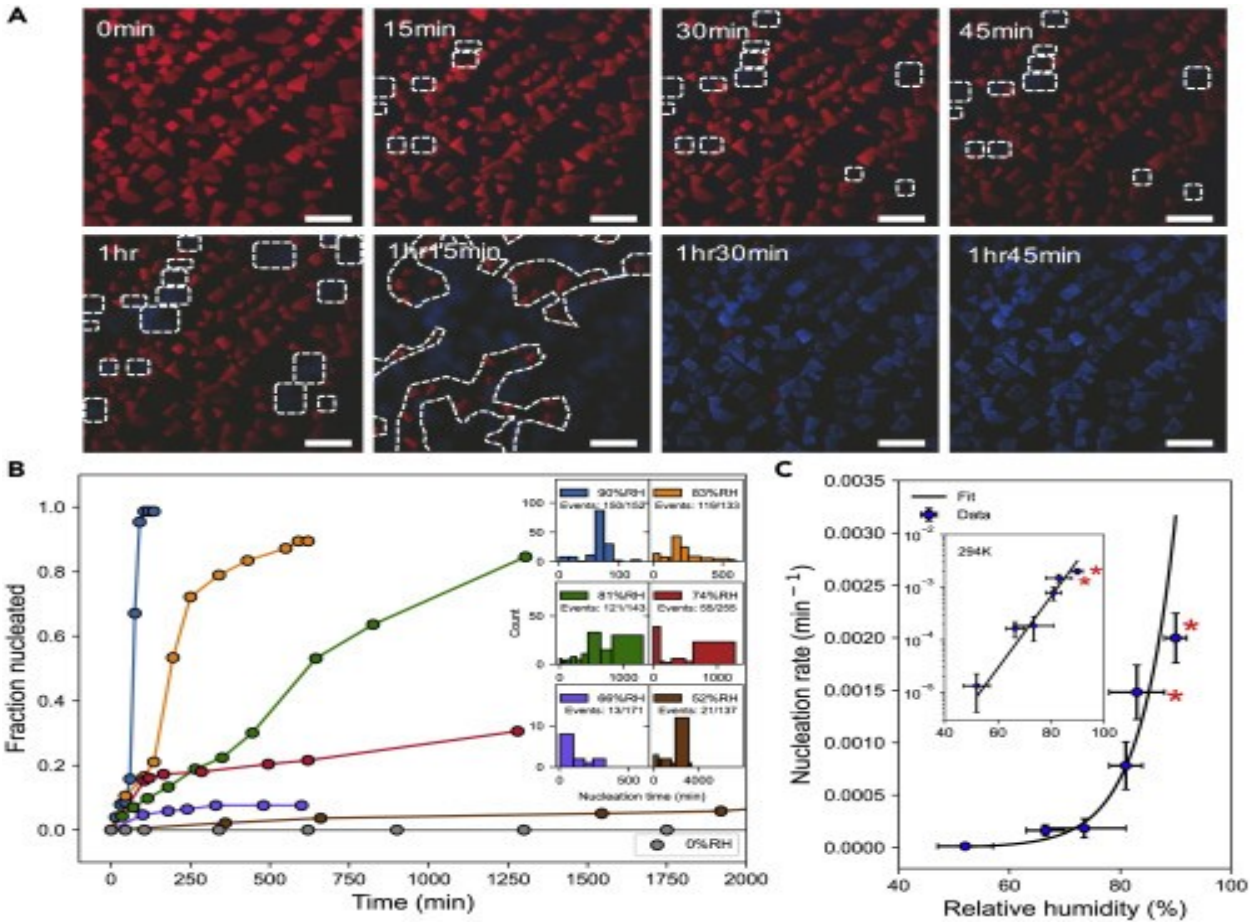

Figure 2. Time evolution of high-T to low-T $CsPbI_3$ phase transformation

(A) PL micrographs of $CsPbI_3$ at 90% RH over time under 375 nm laser excitation. Dotted lines: guide to the eye highlighting the emergence of low-T phase crystals. Scale bars, 20 μm. (B) Distribution of crystal nucleation times (inset) and the corresponding nucleation probability distribution at 0%, 52% (ambient), 66%, 74%, 81%, 83%, and 90% RH.

(C) Dependence of nucleation rate (J_N) on RH. Inset: nucleation rate shown in log plot. Points marked by asterisks are data obtained before microdroplet formation. Nucleation rate value at each RH is averaged over three to four samples. Data are represented as mean ± SD, with horizontal error bars representing fluctuations in RH during incubation.

Following the nucleation of low-T phase, we observed the subsequent growth (experimental procedures/supplemental information) to examine its dependence on the moisture content, and to identify the rate-limiting process in MIPT. The growth of low-T phase completes significantly faster than the time needed to initiate nucleation, and increases weakly with RH in the range of values we considered (45%–85% RH). The growth kinetics was monitored by optical dark-field (DF) imaging due to its benign nature; DF imaging uses scattered visible light that involves a relatively lower energy transfer compared with the incident excitation source used in PL imaging, and therefore can avoid potential laser damage and capture the pristine growth kinetics. Figure 3A compares the PL and DF images of a pristine high-T $CsPbI_3$ plate before and after the transformation. As shown, the DF images depict distinct contrast and thus can be used to track the growth evolution *in situ*. Furthermore, PT-induced cracks are clearly captured using DF due to enhanced light scattering at the boundary and is also evident via scanning electron microscopy (SEM) (Figure 3B). Crack formation can be explained by the relatively large change in crystal volume introduced during the transformation, which results in tension in the untransformed high-T phase region (Figure S8), which eventually leads to plastic deformation.[10] We find that once nucleation begins, the entire high-T crystal (lateral dimension <20 μm) transforms spontaneously into low-T phase in less than a minute, a timescale within which a second nucleation is very unlikely to occur (Figures 3C; Video S2). Within this regime, the “single nucleation” nature statistically eliminates the possibility of an overlap between the growth and any secondary nuclei in the same crystal, allowing us to unambiguously characterize phase growth. Under a fixed RH level, the propagation front proceeds roughly linearly over time (Figure 3D). Comparison of

the phase propagation speed under RH of 45%, 65%, 70%, 75%, and 85% shows that it increases with weakly linear dependence on the moisture level over the range of RH considered, possibly due to halide vacancy-assisted diffusion (Figure 3E). Given its coordinated nature, it is likely that the growth is governed by local tension surrounding the high-T region,[10] or by facile diffusion of the disordered interface.[19] There exists a clear difference between the timescale required to initiate nucleation (10^2–10^4 s) and to complete growth (<60 s). This finding suggests that, in the absence of methods to impede propagation, nucleation is the rate-limiting step in MIPT at room temperature (RT, 20°C). Furthermore, we observed that, when two crystals are attached to each other and share significant surface area, the propagation of one grain can trigger subsequent nucleation and growth of a neighboring grain (Figure S9). A direct translation of this finding into thin film materials, which usually have grain sizes of hundreds of nanometers, would suggest that PT is solely dictated by the nucleation of low-T phase.

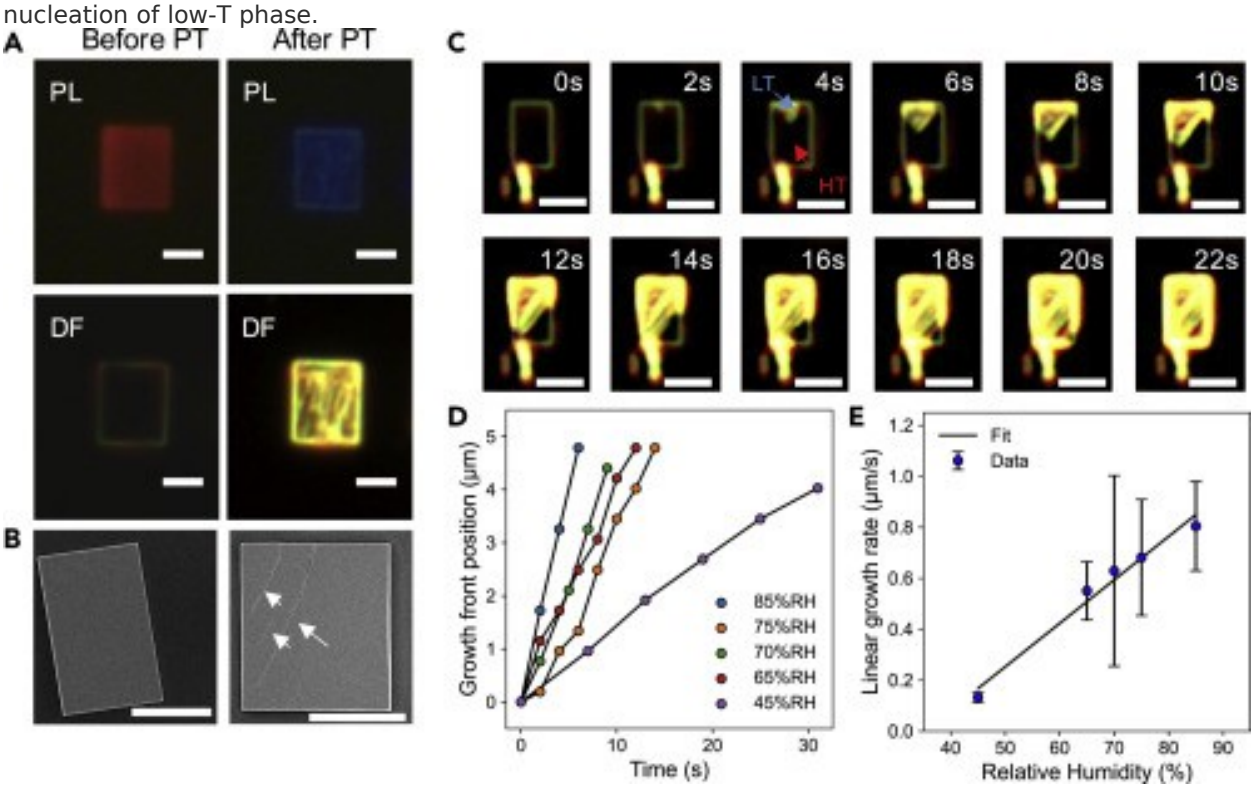

To understand how temperature modifies the PT energy landscapes and extract the associated activation energies, we performed another set of studies under heating and different RH (Figure 4). We chose a small temperature range (RT to 33°C) to minimize shifts in the phase energetics (Figure 1B) to achieve a meaningful extraction of the activation energies. Heating from RT to 33°C increases the nucleation rate under 73% RH and 53% RH (Figures 4A and S10–S11; Table S3). The increase in nucleation rate for 73% RH and 53% RH follows Arrhenius behavior (Figure 4A, inset) described by the classical nucleation theory:[20] $J_N = A*\exp(-E_a/k_BT)$, where J_N, A, E_a, k_B, and T are nucleation rate, kinetic preexponential factor specific to a system, activation energy barrier for nucleation, Boltzmann constant, and temperature, respectively. The extracted E_a is 55.40 ± 3.75 kJ/mol under 73% RH and 129.08 ± 33.86 kJ/mol under 53% RH. We did not observe any nucleation events under inert atmosphere at RT to 35°C within the time frame of the measurement (Figure 4B), an indication of a larger E_a in the absence of moisture and oxygen. The reduction in E_a from 129.08 ± 33.86 kJ/mol under 53% RH to 55.40 ± 3.75 kJ/mol under 73% RH is consistent with previous molecular dynamics calculation[16] that moisture lowers the nucleation barrier.

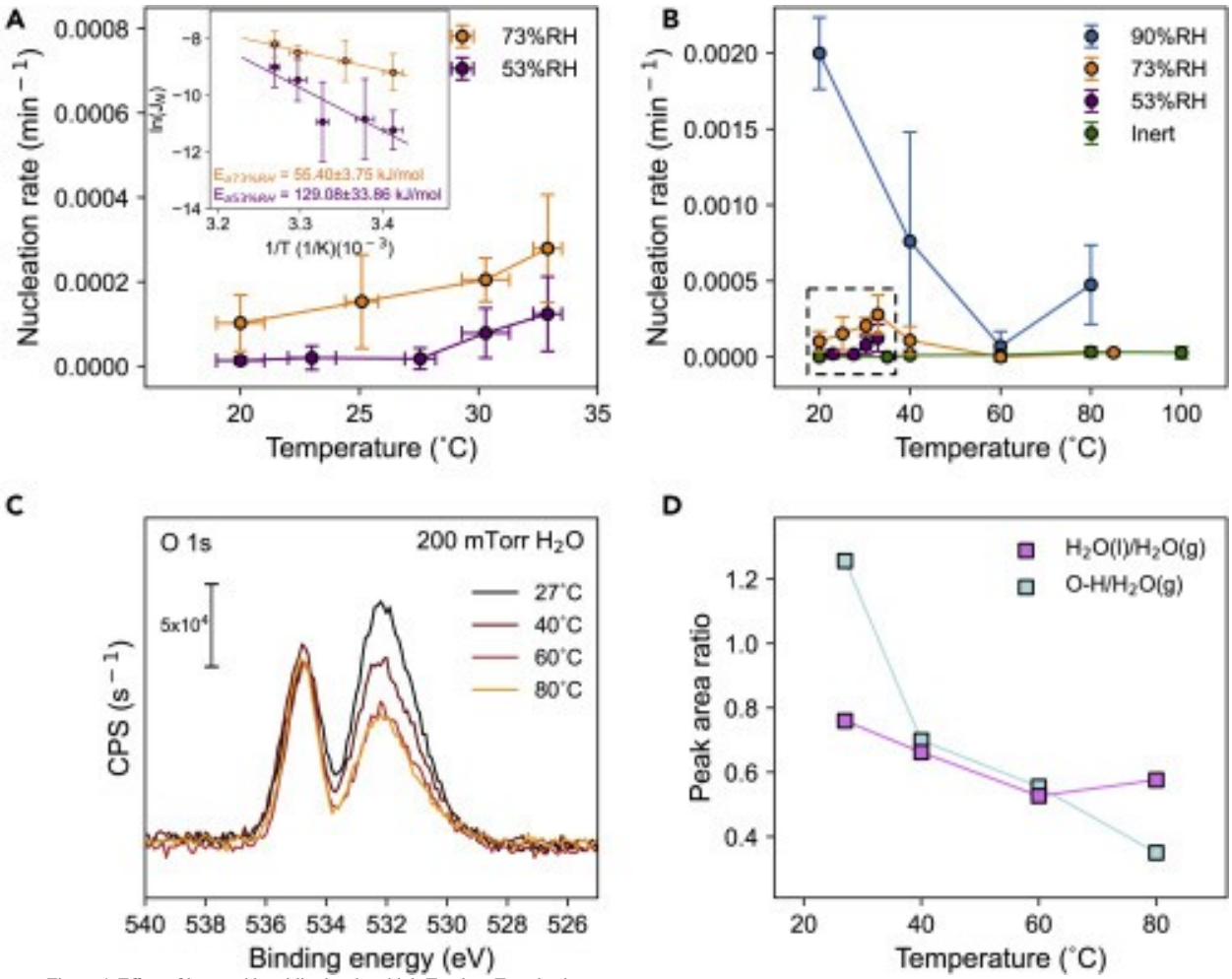

Figure 4. Effect of heat and humidity level on high-T to low-T nucleation

(A) Mild heating at 20°C–33°C increases the nucleation rate under 73% RH and 53% RH. Inset: plot of nucleation rate (J_N) in a logarithmic scale against $1/T$, indicating that the observed trend follows Arrhenius behavior. Data are represented as mean ± SD, with horizontal error bars representing fluctuation in temperature during measurement.

(B) Heating above 40°C under various RH decreases nucleation rate toward that observed under inert atmosphere, due to water desorption evident by AP-XPS measurements in (C and D). Region marked by dotted line is shown in (A). Data are represented as mean ± SD, with horizontal error bars representing fluctuation in temperature during measurement.

(C) O 1s XPS spectra of high-T phase $CsPbI_3$ crystals under 200 mTorr H_2O at various sample temperatures: 27°C, 40°C, 60°C, and 80°C.

(D) Peak area ratio of surface-adsorbed molecular H_2O to gas-phase H_2O (magenta), and surface hydroxyl groups to gas-phase H_2O (cyan). As the temperature is elevated under the isobaric condition (200 mTorr H_2O), the peak area for H_2O(g) (~535 eV) remains stable, while those for H_2O(l) and O-H (~532 eV) decrease, suggesting water desorption from the surface of $CsPbI_3$ crystals (see Figure S15 for detailed peak deconvolution).

We further investigate the nucleation behavior of $CsPbI_3$ under general solar cell operational temperatures ranging from 40°C to 85°C.[6,21] We find that heating at these temperatures reduces the MIPT rate. Comparing nucleation rates obtained from 20°C (RT) to approximately 85°C under 90% RH, 73% RH, and inert atmosphere (Figures 4A and S12–S14; Tables S3 and S4) shows that heating above 40°C in the presence of moisture generally decreases J_N. Under 90% RH, J_N decreases from 2×10^{-3} min^{-1} at RT to 7.61×10^{-4} min^{-1}, 6.96×10^{-5} min^{-1}, and 4.75×10^{-4} min^{-1} at 40°C, 60°C, and 80°C. A similar reduction of J_N is also observed at 73% RH, where J_N decreases from 2.79×10^{-4} at 33°C to 1.07×10^{-4} min^{-1}, 0 min^{-1}, and 2.82×10^{-5} min^{-1} at 40°C, 60°C, and 85°C. To separate the effect of moisture and heat, we placed high-T $CsPbI_3$ under inert atmosphere at 20°C–100°C and found the intrinsic nucleation to be slow (Figures 4B and S14). The nucleation rate at above 40°C for 90% RH and 73% RH tended to approach rates acquired at inert atmosphere, signifying that the effect of moisture is diminished at increased temperature. Heating is known to remove water molecules from both all-inorganic and hybrid perovskite surfaces.[22,23] Thus, we suggest that the decrease in J_N within the temperature range between 40°C and 85°C is due to the water desorption that results in a lower halide vacancy concentration and a higher nucleation barrier. We tested this notion by performing ambient

pressure X-ray photoelectron spectroscopy (AP-XPS) experiments on high-T phase $CsPbI_3$ at elevated temperatures (Figures 4C and S15). As shown in Figure 4C, the O 1s counts near 532 eV associated with adsorbed H_2O and surface O-H continuously decrease at elevated temperature, with no further decrease after 60°C, which supports the experimental observation of nucleation rate as a function of temperature. Comparison of peak area ratios of $H_2O(l)$ to $H_2O(g)$ and O-H to $H_2O(g)$ shows a decrease in O 1s peak area for surface-adsorbed molecular H_2O and surface O-H in Figure 4D, while the peak area for $H_2O(g)$ remains stable, further supporting the hypothesis that water desorbs from the $CsPbI_3$ surface at elevated temperatures. It is notable that while heating at 85°C leads to decomposition in hybrid lead halide perovskites (LHP),[5,6] it stabilizes high-T $CsPbI_3$. These results highlight the enhanced stability of inorganic LHP and suggest that mild heating at 60°C–85°C may be a potentially viable method of stabilizing $CsPbI_3$ and its related compositions to a functional form.

Conclusion

The presence of moisture significantly reduces the stability of $CsPbI_3$ and its related compositions, which consequently hinders their technological application and success. By directly monitoring the high-T to low-T $CsPbI_3$ PT under controlled RH, we are able to quantify the dependence of PT processes on humidity, extract the associated nucleation barriers, and uncover the rate-limiting process. Furthermore, we find heating under general solar cell operating temperature to be a potential method of mitigating MIPT. By providing insight into the effects of environmental factors on phase stability, our work can serve as a reference to thin film applications of $CsPbI_3$ and its related perovskite systems, and lay the groundwork for future designs of stable photovoltaics systems. The imaging techniques described in this report can further be used as a general method to decouple nucleation and growth in materials that exhibit contrasting optical response before and after PT.

Lead contact

Peidong Yang (p_yang@berkeley.edu).

Materials availability

This study did not generate new unique materials.

Synthesis of $CsPbI_3$ microcrystals

The $CsPbI_3$ perovskite crystals were grown by a chemical vapor transport method in a tube furnace (Thermolyne 79,300). The precursor consisting of a 1:1 mole ratio of cesium iodide (99.999% trace metals basis, Aldrich) and lead(II) iodide (99%, Aldrich) was placed at the center of a quartz tube at 500°C, and a Si substrate with 300 nm SiO_2 layer was positioned 13–16 cm from the source. The source was heated from 23°C to 500°C in 10 min, kept at 500°C for another 15 min, cooled down to 330°C in 30 min, kept at 330°C for 3 h, and cooled to RT naturally. Throughout the reaction, high purity N_2 gas (99.998%) was made to flow through the tube at 200 sccm to carry source vapor to the substrate.

Moisture-dependent nucleation rate measurement

The moisture treatment was conducted in a humidity control box with flowing N_2 gas containing moisture. The relative humidity (RH) was controlled in the range 65%–90% using the following protocol. The RH level was measured using a hygrometer (Honeywell). To achieve 65%–70% RH, N_2 was made to flow through water at RT (20°C ± 1°C). To achieve 70%–90% RH, N_2 was made to flow through warm water (60°C–80°C). The warm water vapor resulted in slight condensation on the top and bottom surfaces of the box in the first 30 min. Kimwipes were used to wipe off the water during this time. After the initial 30 min, the water cooled down to a temperature where there is no further condensation. We then waited for the RH level to equilibrize for at least 1 h before starting the moisture treatment. At this time, the temperature of the water was around 30°C–40°C, and the RH level remained at 70%–90% for the duration of the measurement.

The samples were taken out of the moisture box at different time intervals for the PL measurement to track the extent of nucleation. Given that the local RH environment would inevitably start to equilibrize with ambient humidity (52% RH) once the samples were taken out of the box, we performed a control experiment by monitoring the extent of nucleation under 52% RH (Figures 2B and S2E). The number of nucleation events was extremely low at 52% RH compared with that under higher RH levels, which indicated that the number of halide vacancies created at 52% RH was significantly lower than that in higher RH environment. Therefore, we concluded that any additional vacancies created during the time the sample was outside of the box would not significantly affect the overall number of vacancies on the sample surface, and its effect on the overall nucleation trend for higher RH levels would be negligible.

Temperature-dependent nucleation rate measurement in the presence of moisture was achieved by heating the sample on a hotplate under 90% RH, 73% RH, and 53% RH, with temperature calibrated using an IR pyrometer. Temperature-dependent nucleation rate measurement in inert atmosphere was

achieved by flowing ultrahigh purity argon (99.9999%, Praxair) into a sample holder equipped with a heating stage and temperature controller.

Microscopic PL measurement

PL measurement was used to characterize the emission of the sample, which was used to confirm the crystal phase and determine the total number of low-T crystals emerging over time. The microscopic PL characterization was carried out in a PL microscope system. A continuous-wave solid-state laser at 375 nm (Coherent OBIS 375LX) was focused obliquely onto the sample as the excitation source. A laser filter (bandpass, 375 nm/6 nm) was used to clear the laser residual emission. The PL images were collected using a microscope objective (50×, numerical aperture = 0.55) before sending to the grating-based spectrograph (Princeton Instruments, SP-2300i) through an optical fiber for spectrum analysis. A mechanical shutter was used to minimize the laser exposure to the sample. A 390 nm long-pass emission filter was used to filter out the laser signal. The spectrograph was equipped with a diffraction grating of 150 lines/mm (blaze wavelength at 300 nm) and coupled with a CCD detector with optimized detection efficiency by liquid nitrogen cooling to −120°C. The optical image was taken using a CCD camera (Zeiss AxioCam MRc 5).

In situ microscopic DF measurement

An optical microscope (Carl Zeiss) with DF illumination and a microscope objective (50×, numerical aperture = 0.55) was used for *in situ* characterization of the growth. During the characterization, N_2 vapor containing water vapor of various temperatures was flowed through a chamber containing the sample to reach specific RH levels. The RH level was measured using a hygrometer (Honeywell).

In situ AP-XPS measurement

AP-XPS experiments were conducted at the Lawrence Berkeley National Laboratory Advanced Light Source (Beamline 9.3.2). $CsPbI_3$ crystals were grown on highly boron-doped silicon substrates and mounted on a ceramic button heater sample holder to raise the temperature of the sample during experiments. The end station 9.3.2 is equipped with a VG-Scienta R4000 HiPP analyzer, and XPS spectra were collected using an incident X-ray energy of 670 eV under 200 mTorr H_2O. The combined beamline and electron energy analyzer resolution was better than 0.8 eV. Shirley background was used for background subtraction.

Acknowledgments

This work was primarily supported by the U.S. Department of Energy, Office of Science, Basic Energy Sciences, Materials Sciences and Engineering Division under contract no. **DE-AC02-05CH11231 (PChem KC3103**). Ambient pressure X-ray photoelectron spectroscopy (AP-XPS) experiments were conducted with help from E.J. Crumlin and S. Nemsak at the Lawrence Berkeley National Laboratory Advanced Light Source (Beamline 9.3.2), a US DOE Office of Science User Facility under contract no. DE-AC02-05CH11231. Y.Z. acknowledges Suzhou Industrial Park for the fellowship support. J.A.S. acknowledges financial support from the Research Foundation Flanders (FWO: grant nos V439819N and 12Y7221N). S.Y. acknowledges support from Samsung Scholarship. C.K.L. acknowledges MOE Technologies Incubation Scholarship from Taiwan.

Author contributions

Z.L. and P.Y. conceived the idea and designed the study. Z.L. contributed to all experimental work involving optical (PL, DF) and structural (XRD) studies, with helpful discussions from Y.Z., M.G., and J.A.S. Z.L. and Y.Z. performed morphological (SEM) characterization. D.T.L., M.G., and J.A.S. provided insightful discussions on the phase energetics and transformation kinetics of the material systems. Y.Z. synthesized the samples for AP-XPS. S.L. and S.Y. carried out the AP-XPS measurements and the associated data analysis. Y.Z., L.N.Q., and C.-K.L. assisted with the optical measurements. Z.L. and P.Y. wrote the manuscript. All authors have discussed and approved the manuscript.

References

Y. Wang, M.I. Dar, L.K. Ono, T. Zhang, M. Kan, Y. Li, L. Zhang, X. Wang, Y. Yang, X. Gao, *et al.*
Thermodynamically stabilized β-$CsPbI_3$–based perovskite solar cells with efficiencies >18%
Science, 365 (2019), pp. 591-595
CrossRefView Record in ScopusGoogle Scholar
M.V. Kovalenko, L. Protesescu, M.I. Bodnarchuk

Properties and potential optoelectronic applications of lead halide perovskite nanocrystals
Science, 358 (2017), pp. 745-775

View Record in ScopusGoogle Scholar
M.A. Green, A. Ho-Baillie, H.J. Snaith

The emergence of perovskite solar cells
Nat. Photon., 8 (2014), pp. 506-514
CrossRefView Record in ScopusGoogle Scholar
G.E. Eperon, G.M. Paternò, R.J. Sutton, A. Zampetti, A.A. Haghighirad, F. Cacialli, H.J. Snaith

Inorganic caesium lead iodide perovskite solar cells
J. Mater. Chem. A, 3 (2015), pp. 19688-19695
View Record in ScopusGoogle Scholar
B. Conings, J. Drijkoningen, N. Gauquelin, A. Babayigit, J. D'Haen, L. D'Olieslaeger, A. Ethirajan, J. Verbeeck, J. Manca, E. M osconi, *et al.*
Intrinsic thermal instability of methylammonium lead trihalide perovskite
Adv. Energy Mater., 5 (2015), p. 1500477
CrossRefView Record in ScopusGoogle Scholar
L. Shi, M.P. Bucknall, T.L. Young, M. Zhang, L. Hu, J. Bing, D.S. Lee, J. Kim, T. Wu, N. Takamure, *et al.*
Gas chromatography-mass spectrometry analyses of encapsulated stable perovskite solar cells
Science, 368 (2020), p. eaba2412
CrossRefView Record in ScopusGoogle Scholar

A. Swarnkar, A.R. Marshall, E.M. Sanehira, B.D. Chernomordik, D.T. Moore, J.A. Christians, T. Chakrabarti, J.M. Luther

Quantum dot-induced phase stabilization of α-CsPbI3 perovskite for high-efficiency photovoltaics
Science, 354 (2016), pp. 92-95
CrossRefView Record in ScopusGoogle Scholar

M. Lai, Q. Kong, C.G. Bischak, Y. Yu, L. Dou, S.W. Eaton, N.S. Ginsberg, P. Yang

Structural, optical, and electrical properties of phase-controlled cesium lead iodide nanowires
Nano Res., 10 (2017), pp. 1107-1114
CrossRefView Record in ScopusGoogle Scholar

A. Waleed, M.M. Tavakoli, L. Gu, S. Hussain, D. Zhang, S. Poddar, Z. Wang, R. Zhang, Z. Fan

All inorganic cesium lead iodide perovskite nanowires with stabilized cubic phase at room temperature and nanowire array-based photodetectors
Nano Lett., 17 (2017), pp. 4951-4957
CrossRefView Record in ScopusGoogle Scholar

J.A. Steele, H. Jin, I. Dovgaliuk, R.F. Berger, T. Braeckevelt, H. Yuan, C. Martin, E. Solano, K. Lejaeghere, S.M.J. Rogge, *et al.*
Thermal unequilibrium of strained black $CsPbI_3$ thin films
Science, 365 (2019), pp. 679-684
CrossRefView Record in ScopusGoogle Scholar

F. Bai, J. Zhang, Y. Yuan, H. Liu, X. Li, C.-C. Chueh, H. Yan, Z. Zhu, A.K.-Y. Jen

A 0D/3D heterostructured all-inorganic halide perovskite solar cell with high performance and enhanced phase stability
Adv. Mater., 31 (2019), p. 1904735
CrossRefView Record in ScopusGoogle Scholar

F. Ke, C. Wang, C. Jia, N.R. Wolf, J. Yan, S. Niu, T.P. Devereaux, H.I. Karunadasa, W.L. Mao, Y. Lin

Preserving a robust CsPbI3 perovskite phase via pressure-directed octahedral tilt
Nat. Comm., 12 (2021), p. 461
View Record in ScopusGoogle Scholar
S. Dastidar, C.J. Hawley, A.D. Dillon, A.D. Gutierrez-Perez, J.E. Spanier, A.T. Fafarman

Quantitative phase-change thermodynamics and metastability of perovskite-phase cesium lead iodide
J. Phys. Chem. Lett., 8 (2017), pp. 1278-1282
CrossRefView Record in ScopusGoogle Scholar

D.B. Straus, S. Guo, R.J. Cava

Kinetically stable single crystals of perovskite-phase $CsPbI_3$
J. Am. Chem. Soc., 141 (2019), pp. 11435-11439
CrossRefView Record in ScopusGoogle Scholar

R.J. Sutton, M.R. Filip, A.A. Haghighirad, N. Sakai, B. Wenger, F. Giustino, H.J. Snaith

Cubic or orthorhombic? Revealing the crystal structure of metastable black-phase $CsPbI_3$ by theory and experiment
ACS Energy Lett., 3 (2018), pp. 1787-1794

CrossRefView Record in ScopusGoogle Scholar

16

J. Lin, M. Lai, L. Dou, C.S. Kley, H. Chen, F. Peng, J. Sun, D. Lu, S.A. Hawks, C. Xie, *et al.*
Thermochromic halide perovskite solar cells
Nat. Mater., 17 (2018), pp. 261-267
CrossRefView Record in ScopusGoogle Scholar

17

S. Jiang, J.H. ter Horst

Crystal nucleation rates from probability distributions of induction times
Cryst. Growth Des., 11 (2011), pp. 256-261
CrossRefView Record in ScopusGoogle Scholar

18

C.-C. Lin, S.K. Huang, C.-E. Hsu, Y.-C. Huang, C.-Y. Wei, C.-Y. Wen, S.-S. Li, C.-W. Chen, C.-C. Chen

Exploring the origin of phase-transformation kinetics of $CsPbI_3$ perovskite nanocrystals based on activation energy measurements
J. Phys. Chem. Lett., 11 (2020), pp. 3287-3293
CrossRefView Record in ScopusGoogle Scholar

19

C.G. Bischak, M. Lai, Z. Fan, D. Lu, P. David, D. Dong, H. Chen, A.S. Etman, T. Lei, J. Sun, *et al.*
Liquid-like interfaces mediate structural phase transitions in lead halide perovskites
Matter, 3 (2020), pp. 534-545
ArticleDownload PDFView Record in ScopusGoogle Scholar

20

D.A. Porter, K.E. Easterling, M.Y. Sherif

Phase Transformations in Metals and Alloys Ch. 3
CRC Press (2009)
Google Scholar

21

E.J. Juarez-Perez, L.K. Ono, M. Maeda, Y. Jiang, Z. Hawash, Y. Qi

Photodecomposition and thermal decomposition in methylammonium halide lead perovskites and inferred design principles to increase photovoltaic device stability
J. Mater. Chem. A, 6 (2018), pp. 9604-9612
CrossRefView Record in ScopusGoogle Scholar

22

B. Turedi, K.J. Lee, I. Dursun, B. Alamer, Z. Wu, E. Alarousu, O.F. Mohammed, N. Cho, O.M. Bakr

Water-induced dimensionality reduction in metal-halide perovskites
J. Phys. Chem. C, 122 (2018), pp. 14128-14134
CrossRefView Record in ScopusGoogle Scholar

23

A. Halder, D. Choudhury, D. Ghosh, A.S. Subbiah, S.K. Sarkar

Exploring thermochromic behavior of hydrated hybrid perovskites in solar cells
J. Phys. Chem. Lett., 6 (2015), pp. 3180-3184
CrossRefView Record in ScopusGoogle Scholar

z